Hindawi
Journal of Engineering
Volume 2022, Article ID 4428060, 17 pages
https://doi.org/10.1155/2022/4428060

Research Article

Conjugate Natural Convection: A Study of Optimum Fluid Flow and Heat Transfer in Eccentric Annular Channels

Ahmad Jamal [1] **and Esmail M. A. Mokheimer** [2]

[1]*Mechanical Engineering Department, Jubail University College, Jubail 31961, Saudi Arabia*
[2]*Mechanical Engineering Department, King Fahd University of Petroleum and Minerals, Dhahran 31261, Saudi Arabia*

Correspondence should be addressed to Ahmad Jamal; jamalah@ucj.edu.sa

Received 24 November 2021; Accepted 8 February 2022; Published 3 March 2022

Academic Editor: Abdullah A. Kendoush

Laminar natural convection-conduction heat transfer in vertically positioned annular channels with inherent eccentricity is investigated for optimum solid-fluid thermal conductivity ratio and optimum cylinder walls thicknesses allowing maximum induced fluid flow rate and heat transfer under varying geometry parameters, i.e., annulus eccentricity and radius ratio. A finite-difference technique is employed to solve the coupled momentum and energy equations for the cylindrical annulus walls and the annular fluid with Prandtl number 0.7. As part of the results, fluctuations in the induced fluid flow rate and heat transfer in the eccentric annular channel due to the conjugate effect, governed by the ratios of the solid and fluid thermal conductivities and thicknesses of outer and inner circular cylinder walls, are obtained for the boundary conditions of one wall heated isothermally and the other kept adiabatic. Commonly encountered ratios of the solid and fluid thermal conductivities and cylinder walls thicknesses are utilized in the present analysis. Results reveal that the optimum conductivity ratio and cylinder walls thicknesses increase nonlinearly with eccentricity and radius ratio. Such results can be very useful in effectively designing the heat transfer equipment for optimum performance.

1. Introduction

Combined conduction-natural convection (conjugate) heat transfer in vertically positioned annular channels with eccentricity finds various applications in the passive cooling of electrical parts, nuclear power plants, oil and gas drilling components, etc. One of the applications is the cooling of electric power cables. Each inner small cable (the inner cylinder) is positioned eccentrically into the outer housing (the outer cylinder). Heat is generated in the copper wire due to the flow of electricity. This generated heat must be dispensed to the outer surrounding. In general, the only source of heat dissipation is the natural convection in which the heat reaches the annular gap between the cable and the outer housing by passing through the covering of each cable and then passing through the outer housing to the surrounding.

Substantial work has been done to investigate conjugate heat transfer in different geometrical domains. The effect of tube wall axial heat conduction on steady-state laminar convection heat transfer of a fluid in a single-phase within the tube with a step shift in the heat flux was numerically investigated by Anand and Tree [1]. The effect of wall thermal conduction on natural convection flow and heat transfer between two unevenly heated upright panels with heat flux was examined numerically by Kim et al. [2]. A finite-difference implicit scheme was utilized to resolve the governing equations of the phenomenon. They took into account various independent parameters influencing wall conduction, such as the ratio of solid and fluid thermal conductivities, the asymmetric heating parameter, channel height-width ratio, wall thickness-channel width ratio, and Grashof number. Chung [3] investigated combined conduction-natural convection in a power-law (non-Newtonian) fluid in a vertically positioned thick channel with separate sources of heat in both the channel walls and the fluid using the finite-difference technique. Sheremet [4]

developed a mathematical model of unsteady three-dimensional combined conduction-natural convection in a closed vertically positioned cylindrical channel dissipated to its surroundings with a local heat source. Hassab et al. [5] developed a finite-difference technique to solve the combined conduction-laminar forced convection in a parallel-plate channel with two different coolant fluids. They showed that the conjugate effect could be enhanced by significantly changing the parameters such as coolant fluids' temperature difference step change, Biot number, and wall thickness ratio.

Numerous research papers are found on conjugate forced/free convection in concentric annular channels. El-Shaarawi et al. [6] proposed a finite-difference-based numerical model to address the unsteady conduction-forced convection problem in an annular channel formed by two concentric cylinders with concurrent development of thermal and hydrodynamic boundary layers. With a finite-difference scheme, El-Shaarawi et al. [7] numerically studied the unsteady conduction-forced convection in a concentric annular channel full of an isotropic and homogeneous porous medium. El-Shaarawi and Negm [8, 9] investigated the steady and unsteady conduction-laminar natural convection heat transfer in vertically positioned concentric annular channels open at both ends using a computational model based on the finite-difference method. Aldoss et al. [10] studied the influence of a medium with considerable porosity on steady-state combined conduction-free convection flow and heat transfer in an annular channel bounded by two concentrically aligned horizontal cylinders. Imtiaz and Mahfouz [11] utilized the Fourier Spectral Method (FSM) to numerically analyze flow driven by buoyancy effect and combine conduction-convection flow and heat transfer in a concentric annular channel full of micropolar fluid. More recently, a numerical study on conjugate natural convection in a horizontally placed concentric annular channel using Carreau non-Newtonian blood as the annular fluid was conducted by Alsabery et al. [12]. According to them, natural convection flow and heat transfer in the flow of blood using the Carreau model attracted fewer researchers in the past. They incorporated the finite element technique to solve the equations governing the conjugate natural convection phenomenon.

Despite several studies published in the past for traditional cases of either free or forced convection in eccentric annular channels [13–25], a close examination of the literature revealed that there are limited research articles available related to the combined conduction-convection case in vertical/horizontal eccentric annular channels. One of those is that of El-Shaarawi and Haider [26] for the case of forced flow convection. They obtained the results for a fluid having a Prandtl number equal to 0.7 flowing with eccentricities 0.1, 0.3, 0.5, and 0.7 in a fluid annular channel with a nondimensional radius ratio equal to 0.5. The other articles by El-Shaarawi et al. [27, 28] numerically studied the effects of conduction-convection coupling (conjugation) and geometry parameters on steady-state laminar flow natural convection in vertically positioned open-ended annular channels with inherent eccentricity. An article by Jamal et al. [29] presented numerical results of critical threshold values of the ratio of solid and fluid thermal conductivities beyond which, and walls thicknesses under which, the conjugate effect on natural convection flow and heat transfer in vertically positioned eccentric annular channels bounded by the finite thicknesses of outer and inner circular cylinder walls could be neglected. In a recent article, Nasiri et al. [30] studied the steady-state conjugate natural convection in an infinitely long horizontal eccentric annular channel by employing the SIMPLER algorithm of the finite volume method. They considered the finite thickness of only the inner wall of the cylinder and studied the effects of solid-fluid conductivity ratio, eccentricity, the thickness of inner cylinder wall, and the angular location of the inner cylinder relative to the outer one on combined conduction-natural convection flow and heat transfer.

Here, it is important to include some accounts of the experimental work on natural/forced convection in vertical concentric/eccentric annular channels. In 1990, El-Genk and Rao [31] published a paper in which they did laminar flow visualization of water flow and heat transfer measurements in a vertically positioned concentric annular channel having the inner heated annular channel wall and outer insulated wall. Later, Takahashi et al. [32] carried out experimental and numerical methods to study the natural/free convection phenomenon in a vertical concentric annular channel filled with air for different thermal boundary conditions, inner to outer pipe diameter ratios, and modified Grashof numbers. They measured and analyzed thermally developing as well as fully developed regions. Investigation on natural convection in a vertically positioned eccentric annular channel with open ends was done by Hosseini et al. [33], in which they kept the outer annular channel wall heated whereas the inner one adiabatic and varied the eccentricity and uniform heat flux to find optimum eccentricity at which maximum heat transfer coefficient in the annular channel filled with air could be obtained. Husain and Siddiqui [34] used an experimental set-up by partially heating the inner annular channel wall with varying heat flux to investigate the natural convection flow and heat transfer in a high aspect ratio (annular length to gap ratio) vertical concentric annular channel having water as the annular working fluid. In addition to this, their work included numerical simulation and comparison of the results with those obtained from experiments. The effect of rotating outer unheated cylinder with varying rotation parameters (ratio of Reynolds and Grashof numbers) on the natural convection air draft induced in the vertically positioned concentric annular channel due to the inner stationery heated cylinder was studied both experimentally and numerically by Chithrakumar et al. [35]. A recent paper is by Zhu et al. [36] in which they investigated forced convection in vertically positioned eccentric annular channels experimentally and numerically under varying water-air working fluid ratio, eccentricity, and radius ratio with constant incoming volumetric flow rate. In all the above experimental studies, the conjugate effect was not considered.

The present paper explores a very important aspect of the coupled conduction-natural convection phenomenon in

vertically positioned eccentric annular channels, i.e., optimum solid-fluid thermal conductivity ratio and optimum cylinder walls thicknesses, for a set of boundary conditions not previously applied on the cylinder walls for the conjugate case. A finite-difference technique-based numerical model is used to solve the conjugate natural convection case. Numerical results are obtained for the variation of the fluid flow rate induced in the eccentric annular channel and convective heat transfer influenced by the conjugate effect under the thermal boundary conditions of isothermally heating one cylinder wall while keeping the other adiabatic, also known as boundary conditions of the third kind. Finally, the optimum values of thermal conductivity ratio and walls thicknesses with maximum induced fluid flow rate and convective heat transfer for given eccentricities and radius ratios are obtained.

2. Problem Formulation

The present problem consists of a vertical eccentric annular channel. Fluid enters the annular channel and flows upward by natural convection due to a density gradient that is generated as a consequence of the thermal boundary conditions imposed on the annular cylinder walls. Two cases can be considered. One is termed case I, in which the isothermal heating is applied on the inner side of the inner cylinder while the outer side of the outer cylinder is kept adiabatic, whereas the other is termed case O, in which these boundary conditions are swapped. A typical application of the swappable boundary conditions can be found in the case of a sectioned curved double glass window with air filled in the gap between the two layers of glass. A coating with low thermal emissivity is added between the layers. During summer, the outer surface of the outer glass is at high temperature while the inner surface of the inner glass, with the help of the coating, is at low temperature and represents a low conductivity surface that can be idealized as insulated. On the other hand, the inner surface of the inner glass remains at high temperature as compared to the outer surface of the outer glass in winter. Again the outer glass with the coating is not supposed to let the heat escape through it and can be idealized as insulated. The current numerical model is capable of simulating this scenario by entering a very low nondimensional eccentricity such as 0.01. The partial differential equations (PDEs) representing the fluid flow and heat transfer through a geometrically eccentric fluid annular channel are expressed in the bipolar coordinates. On the other hand, the cylindrical coordinates are more suitable for the cylindrical solid walls because of their uniform thickness and circular curvature. Therefore, the heat conduction equations for the cylindrical walls are represented in the cylindrical coordinate system. Figure 1 depicts the bipolar and cylindrical coordinate systems.

Due to the geometrical symmetry about the x-axis as can be seen in Figure 1, half of the symmetric geometry, i.e., $0 \le \xi \le \pi$, is considered for analysis. Hughes and Gaylord [37] presented the equations governing fluid flow and heat transfer in a general form of orthogonal curvilinear

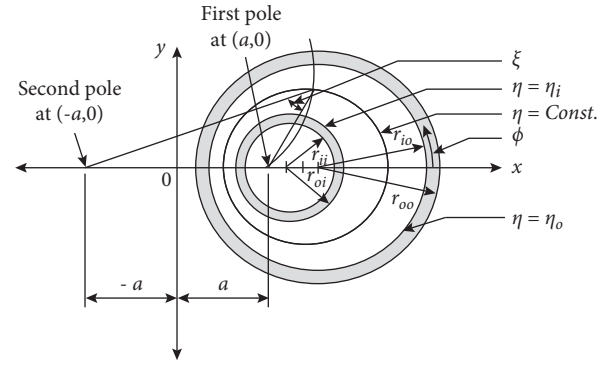

Figure 1: Bipolar and cylindrical coordinate systems in a 2D cross section of the geometry.

coordinate system. The fluid is considered as Newtonian. In case of non-Newtonian fluids, when shear is applied, their viscosity decrease or increase, depending on the fluid. So if a non-Newtonian fluid is used in the eccentric annulus, the shear thickening or shear thinning effects must be considered. Specifically, in case of shear thickening, the increasing viscosity with shear might result in modified convective flow patterns and effect the heat transfer. In order to use a non-Newtonian fluid for such problems, different non-Newtonian fluid models must be used in addition to the above consideration. The steady laminar fluid flow goes into the open-ended vertical eccentric annular channel from its bottom with a flat velocity profile U_o. The assumption of a uniform inlet velocity is a widely used inlet velocity profile for the natural convection flows [8, 9, 18, 19, 38–41]. Hydrodynamic and thermal boundary layers then simultaneously develop as the flow progresses vertically in the channel. Furthermore, to simplify the equations, certain parabolic-flow assumptions [42] are considered. These simplifying assumptions are as follows: the pressure is defined solely by the axial (vertical) coordinate ($\partial p/\partial \eta = \partial p/\partial \xi = 0$), the momentum and energy axial diffusions in the entire domain, including eccentric fluid annular channel and cylinder walls, are ignored ($\partial^2/\partial z^2 = 0$), and the component of η-velocity (v) is significantly lesser than the components of ξ- and z-velocity (w and u). A steady-state solution is obtained with the thermal boundary conditions uniformly imposed along the total length of the outer and inner sides of the circular cylinder walls making the axial (z-direction) conduction (diffusion of energy) in cylinder walls negligible. Moreover, the axial momentum in the annular fluid is mainly by convection and not by diffusion. Hence, ignoring axial diffusion of energy and momentum in the entire domain is a reasonable assumption. The present numerical model is formulated for laminar flow only. Turbulent flow has high irregularity, diffusivity, rotationality, and energy dissipation. In the present model, the simplifying assumptions, as indicated above, make the model suitable for steady-state laminar flows. The other reason for not considering the turbulent flow is that the natural convection is density gradient driven heat transfer and the flow velocities are very low and seldom reach the turbulent flow regime.

Using the dimensionless parameters presented in the nomenclature, carrying out the magnitude analysis of the individual terms of the equations, and considering that the above simplifying assumption justifies the removing of the η-momentum equation, the equations for a steady-state flow with no radiation heat transfer, no dissipation of energy due to viscous effects, and no internally generated heat, and with body force (due to buoyancy) in only the vertical direction can be expressed as follows [27].

2.1. Continuity Equation

$$\frac{\partial(HV)}{\partial\eta}+\frac{\partial(HW)}{\partial\xi}+4\left(1-\chi_2\right)^2\frac{\partial\left(UH^2\right)}{\partial Z}=0. \tag{1}$$

2.2. Z-Direction Momentum Equation

$$\frac{V}{H}\frac{\partial U}{\partial\eta}+\frac{W}{H}\frac{\partial U}{\partial\xi}+4\left(1-\chi_2\right)^2U\frac{\partial U}{\partial Z}=\frac{\theta}{4\left(1-\chi_2\right)^2}-\frac{1}{4\left(1-\chi_2\right)^2}\frac{\partial P}{\partial Z}+\frac{1}{H^2}\left(\frac{\partial^2U}{\partial\eta^2}+\frac{\partial^2U}{\partial\xi^2}\right). \tag{2}$$

2.3. ξ-Direction Momentum Equation

$$\frac{V}{H^2}\frac{\partial(HW)}{\partial\eta}+\frac{W}{H}\frac{\partial W}{\partial\xi}-\frac{V^2}{H^2}\frac{\partial H}{\partial\xi}+4\left(1-\chi_2\right)^2U\frac{\partial W}{\partial Z}=\frac{1}{H^3}\left[\frac{\partial^2(HW)}{\partial\eta^2}+\frac{\partial^2(HW)}{\partial\xi^2}\right]-\frac{2}{H^4}\left[\frac{\partial(HW)}{\partial\eta}-\frac{\partial(HV)}{\partial\xi}\right]\frac{\partial H}{\partial\eta}+\frac{8\left(1-\chi_2\right)^2}{H^2}\frac{\partial H}{\partial\xi}\frac{\partial U}{\partial Z}. \tag{3}$$

2.4. Fluid Energy Equation

$$\frac{V}{H}\frac{\partial\theta}{\partial\eta}+\frac{W}{H}\frac{\partial\theta}{\partial\xi}+4\left(1-\chi_2\right)^2U\frac{\partial\theta}{\partial Z}=\frac{1}{\mathrm{Pr}H^2}\left(\frac{\partial^2\theta}{\partial\eta^2}+\frac{\partial^2\theta}{\partial\xi^2}\right). \tag{4}$$

2.5. Cylinder Walls Energy Equation

$$\frac{\partial^2\theta_s}{\partial R^2}+\frac{1}{R}\frac{\partial\theta_s}{\partial R}+\frac{1}{R^2}\frac{\partial^2\theta_s}{\partial\phi^2}=0. \tag{5}$$

For the outside cylinder wall, $\theta_s=\theta_{so}$ and R vary from $\chi_3=1$ to χ_4

For the inside cylinder wall, $\theta_s=\theta_{si}$ and R vary from χ_1 to χ_2.

2.6. Continuity Equation Integral Form. The integral form of the continuity equation (1) with no-slip (zero velocity) conditions at the annular walls is as follows:

$$\overline{U}=\frac{8\left(1-\chi_2\right)}{\pi\left(1+\chi_2\right)}\int_0^{\pi}\int_{\eta_o}^{\eta_i}UH^2\mathrm{d}\eta\mathrm{d}\xi. \tag{6}$$

Here U, V, and W are the nondimensional velocities in the axial, η-, and ξ-directions, H is the nondimensional scale factor for coordinate transformation, χ_2 is the radius ratio, θ is the nondimensional temperature, P is the nondimensional fluid pressure at any cross section of the annulus, Pr is the Prandtl number, R and ϕ are the first and second transverse cylindrical coordinates in the radial and tangential directions, respectively, and $\overline{U}$ is the nondimensional average axial velocity. The fluid entering the eccentric annulus under natural convection is considered to obey the Boussinesq approximation, according to which the flow has a considerable temperature triggered density gradient in the body force term of the axial momentum equation. Due to this, the pressure in the axial direction varies significantly more than in other transverse directions. Moreover, dropping of $\partial p/\partial\eta$ and $\partial p/\partial\xi$ is justified by the fact that while carrying out the order of magnitude analysis of the governing equations, the pressure terms resulted in the lower order of magnitude than the other terms in the η- and ξ-momentum equations. It is to be noted that due to the lower order of magnitude of the η (radial-like)-velocity component than the ξ (azimuthal-like)- and Z (axial)-components of fluid velocity, the η-momentum equation is dropped. As a matter of fact, in concentric annular channels, the velocity component in the radial direction is not zero in the hydrodynamic developing region, whereas the azimuthal velocity component is zero. In eccentric annular channels with little eccentricity, η- and ξ-velocity components are essentially nonzero. However, these are of a much lower order of magnitude than the Z-component of the fluid velocity U in the developing region. With the increase of eccentricity, the ξ-component of the fluid velocity W becomes more profound than the η-component of the fluid velocity V and becomes significant. One should not infer from dropping the η-momentum equation that there is no velocity component V in the mathematical model; it simply means that its order of magnitude is lower than the other two components of the fluid velocity, i.e., U and W (velocity component V can be seen in equations (1)–(4)).

The following boundary conditions are applied to equations (1) through (5):

(i) $U = U_o$, $W = V = 0$, and $P = -U_o^2/2$ for $Z = 0$ and $\eta_i > \eta > \eta_o$

(ii) $P = 0$ for $Z = L$ and $\eta_i > \eta > \eta_o$

(iii) $U = V = W = 0$ for $Z \geq 0$ and $\eta = \eta_i$ and η_o

(iv) $\theta_{si} = 1$ and $\partial\theta_{so}/\partial R = 0$ for case I, and $\partial\theta_{si}/\partial R = 0$ and $\theta_{so} = 1$ for case O

(v) At the line of symmetry ($\xi = 0$ and π and for $Z > 0$):

$$\frac{\partial U}{\partial \xi} = \frac{\partial V}{\partial \xi} = \frac{\partial W}{\partial \xi} = \frac{\partial \theta}{\partial \xi} = \frac{\partial \theta_s}{\partial \phi} = 0, \tag{7}$$

(vi) At the outer and inner interfaces ($R = \chi_3$ ($\chi_3 = 1$) and χ_2 and for $Z > 0$)

$\theta_f = \theta_s$, continuity of temperature, and $(1/H)((\partial\theta/\partial\eta) + (\partial\theta/\partial\xi)) = K_r((\partial\theta_s/\partial R) + (1/R)(\partial\theta_s/\partial\phi))$, continuity of heat flux

Here U_o is the nondimensional axial velocity at the annulus entrance. It is observed in the mathematical model that the pressure gradient in Z-direction is of first-order, i.e., $\partial P/\partial Z$. Therefore, only one boundary condition is needed for pressure, which is $P = -U_o^2/2$ at $Z = 0$. Here, it is important to mention that the boundary condition for the pressure is given in the dimensionless form. As can be seen in the nomenclature, the expression for U_o involves kinematic viscosity γ, which is μ/ρ. In addition, the Grashof number is also a function of density ρ. Hence, ρ is inherent in the expression of U_o and does not need to be included explicitly in the expression of dimensionless pressure boundary condition.

3. Numerical Solution Steps

Equation (5) is written two times; once for the outer cylinder wall and the second time for the inner one. That makes seven equations. The present problem has seven unknown parameters; the three components of fluid velocity U, V, and W, pressure P, the temperature field in the fluid eccentric annulus θ_f, and the temperatures in both the cylinder walls θ_{si} and θ_{so}. The above governing equations are transformed into finite-difference forms, obtained by El-Shaarawi et al. [27], to solve the seven unknowns at the gridline intersections, i.e., nodes, for each axial (vertical) location Z. The solution continues in exponentially increasing axial steps from the entrance to the exit of the channel. The thermal properties of the annular channel interfaces such as temperature and heat flux are unknown because boundary conditions are applied on the outer and inner sides of the outer and inner cylinder walls, respectively. Also, using the eccentric annular channel governing equations and the heat conduction equations for the cylinder walls in bipolar and cylindrical coordinate systems, respectively, results in unparalleled nodes on both annular channel interfaces. To cater for this mismatch, continuity of temperature and continuity of heat flux principles are used to obtain the temperature values on the cylindrical grid nodes at the annulus interfaces, whereas linear interpolation relations are used to obtain the temperature values on the bipolar grid nodes at the annulus interfaces. Hence the aforesaid problem is treated as a coupled problem.

For any heat transfer problem, the channel dimensions (channel height l and hydraulic diameter D_h), wall thermal boundary conditions, and surrounding temperature are generally known while the induced flow rate f (nondimensional flow rate F) is not known. Conversely, the current problem is treated oppositely, i.e., the unknown nondimensional channel height L is calculated for a given nondimensional induced flow rate F while checking the pressure condition of $P = 0$. Satisfaction of this condition of pressure ($P = 0$) marks the channel exit and hence the channel height, i.e., $Z = L$. Hence, the pressure condition at the channel exit is a check rather than a boundary condition. The present investigation considers seven nondimensional parameters, namely, the Prandtl number Pr, inlet velocity of fluid U_o, ratio of solid and fluid thermal conductivities K_r, the eccentricity E, the annular channel radius ratio χ_2, and the outer and inner cylinder walls thicknesses δ_o and δ_i. These parameters control conjugate natural convection phenomenon in the eccentric annular channel. Here, it is worth mentioning that the general relation of dimensional eccentricity in a bipolar coordinate system can be extracted from the article by Akyildiz et al. [43]. The expression can be expressed as $e = a(\coth \eta_o - \coth \eta_i)$. While converting this dimensional eccentricity to a nondimensional form, the annular gap is taken as the reference, which remains constant at any given angle in the domain. Thus the nondimensional form is expressed as $E = e/(r_{io} - r_{oi})$. For the radius ratio, it is known that the size of a circular channel or pipe is given by its nominal pipe size, which is its inner diameter [44]. Therefore, the inner radius of the outer cylinder is taken as the reference dimension and the nondimensional from the annular gap is obtained by dividing the outer radius of the inner cylinder by the reference given as $\chi_2 = r_{oi}/r_{io}$.

The solution proceeds step by step. First, for a given Prandtl number and geometry parameters, the values of η_i and η_o are computed. The values of $\Delta\eta$ & $\Delta\xi$ are then determined by choosing a reasonable number of intervals in the directions of η and ξ (N and M, respectively). Similarly, ΔR_o, ΔR_i, and $\Delta\phi$ are determined for the cylinder walls by choosing reasonable values of χ_1 and χ_4, an appropriate number of radial intervals in the outer and inner cylinder walls NSO and NSI, and also an appropriate number of intervals in the circumferential ϕ direction M. Uniform inlet axial velocity U_o is assumed. The corresponding nondimensional induced fluid flow rate F is then found by means of the relation $F = U_o(1 - \chi_2^2)$.

The governing equations in finite-difference forms (1) through (6) are solved for the present problem. At each axial location, the unknown parameters θ_f, θ_{si}, and θ_{so} are determined at the next axial location by solving equations (4) and (5) together through Gauss-Seidel iteration. Inside the Gauss-Seidel iteration, the two interface node temperatures of the cylindrical grid are determined with the help of the principles of the continuity of temperature and heat flux, whereas the two interface node temperatures of the bipolar grid are determined by performing linear interpolation

among the cylindrical grid node temperatures surrounding the bipolar grid nodes. To determine the two unknown parameters P and U at each axial (vertical) location, equations (2) and (6) are used. The resulting equations from the application of equation (2) at each annular channel interior grid node along with that equation resulting from expressing the integral continuity equation using the trapezoidal rule are put in a matrix form. This matrix form of the system of equations is resolved using a modified form of the Gauss-Jordan elimination technique, which was previously used by El-Shaarawi [45]. To compute the W-velocity component, the tangential ξ-momentum equation (3) is solved by means of Gauss-Seidel iteration. Finally, the V-component of the fluid velocity at all the annular grid inner nodes is evaluated by solving the continuity equation (1). These computational steps are repeated at each advancing axial (vertical) location until the pressure condition becomes zero ($P = 0$), marking the channel exit.

4. Results and Discussion

The Grashof number is not explicitly needed for the solution process since it is embedded in the nondimensional equations of the problem. Convective heat transfer and fluid flow phenomena, during the computational analysis, are investigated for different values of nondimensional eccentricity ($E = 0.1, 0.3, 0.5, 0.7$) and the ratio of annular channel radii ($\chi_2 = 0.1, 0.3, 0.5, 0.7$) to obtain values termed as optimum conductivity ratio $K_{r,\text{opt}}$ and optimum walls thicknesses $\delta_{i,\text{opt}}$ and $\delta_{o,\text{opt}}$, allowing maximum induced flow rate F and total heat absorbed $\overline{Q}$ in the eccentric annular fluid for the above-mentioned geometry parameters. Here, δ_i is fixed at half of the value of δ_o according to the practical ranges of these parameters. Standard practical outer and inner walls thicknesses and solid-fluid thermal conductivity ratios [27] are used in the present analysis.

Numerical discrepancies can be lessened by increasing the number of grid nodes or, in other words, reducing the size of the mesh. In order to obtain a grid-free solution, twelve separate sizes of the mesh for the fluid annular channel and outer and inner cylinder walls are tried. Summary of some of those for the selected parameters is shown in Table 1. The parameters $\overline{HF}^{1.I}_{i,\text{ex}}$ and $\overline{HF}^{1.I}_{o,\text{ex}}$ are the nondimensional heat fluxes averaged on the inner and outer cylinder walls at the channel exit, $\overline{Nu}^{1.I}_{i,\text{ex}}$ and $\overline{Nu}^{1.I}_{o,\text{ex}}$ are the Nusselt numbers averaged inner and outer cylinder walls at the channel exit, and $\theta^{1.I}_{m,\text{ex}}$ is the dimensionless mean bulk temperature at the channel exit. Case 1. I represents the boundary condition of the first kind, which is obtained by isothermally heating the inner side of the inner cylinder wall while keeping the outer side of the outer cylinder wall at the temperature of inlet fluid (ambient). On the other hand, Case 1. O is obtained by interchanging these boundary conditions between the cylinder walls. Combinations of 30 divisions in η- and ξ-directions in the eccentric annular channel and 30 divisions in R- and ϕ-directions in the cylinder walls are taken as reference mesh sizes. After running the computer code for all mesh sizes, grids of 25 divisions in η- and ξ-directions in the fluid annular channel and 25 divisions in each R- and ϕ-directions in the cylindrical walls are selected. These mesh sizes represent an acceptable percentage difference (<0.2%) of the selected parameters from the reference mesh values and reasonable computational time. Moreover, the standard dimensions of outer and inner tubes presented by El-Shaarawi et al. [27] indicate that the outer wall thickness is almost double that of the inner one.

Based on this proportion, two mesh combinations in R-direction for the outer and inner cylinder walls are further tested as shown in Table 2. It is evident from the results of the selected parameters that the mesh combination of 20 & 10 segments in R-direction in the outer and inner cylinder walls, respectively, provides a good compromise between percentage difference of parameter values (<0.4%) from those of reference mesh size, i.e., 25 & 25 segments and the code execution time. Hence, the outer and inner cylinder walls mesh sizes in R- and ϕ-directions become 20×25 and 10×25, respectively.

The adequacy of the present numerical model is established through special runs of FORTRAN computer code capable of solving conventional (without conjugation, $K_r \longrightarrow \infty$) and conjugate cases of both forced and natural convection. Forced convection can be simulated in the present computer code when the inlet velocity of fluid flow U_o surpasses the inlet velocity for natural convection [42]. In the code, to simulate the conventional cases, the ratio of solid and fluid thermal conductivities is increased ($K_r = 1000$) while cylinder walls thicknesses are decreased ($\delta_o = 0.002$ and $\delta_i = 0.001$) substantially. The outcomes of these special computer runs are presented below.

First, the present numerical model is validated through simulating conventional natural convection in the concentric annular channel and comparing the results of local Nusselt number NU_i varying along the heated inner cylinder wall in the axial (vertical) direction with those obtained experimentally by Takahashi et al. [32] at a modified Grashof number $\text{Gr}* = 5.1 \times 10^3$. They used a stainless-steel inner heated cylindrical pipe and a heatproof vinyl resin outer cylindrical pipe. They also wrapped the outer pipe with an insulating material to minimize the heat loss through it, thus making it an adiabatic wall. They considered the ratio of the diameters of the inner and outer cylindrical pipes as d_i/d_o $(\chi_2) = 0.64$. The concentricity of the cylinders in the present theoretical model is achieved by taking a very small value of $E = 0.01$. Figure 2 shows numerical model results in good agreement with the experimental ones.

Secondly, the present code is run to simulate the results of conventional fully developed forced convection to compare with those obtained by Trombetta [13], El-Shaarawi and Haider [26], and Shah and London [46]. $(\text{d}p/\text{d}z)_{fd}$ is the fully developed pressure gradient and $\overline{HF}^{1.I}_{i,f\ d}$, $\overline{Nu}^{1.I}_{i,f\ d}$, and $\overline{Nu}^{1.I}_{o,f\ d}$ are heat flux and Nusselt numbers at the inner and outer annulus interfaces in the fully developed region. Thermal boundary conditions of first kind Case 1. I are imposed on the cylinder walls. The comparison is shown in Table 3 below. It is observed that 0.363%, 0.124, and 1.348% are the maximum discrepancies between the present computer code outcomes and those obtained by Trombetta, El-Shaarawi, and Haider, and Shah and London, respectively.

Table 1: Summary of mesh-independence test in eccentric annuls and cylinder walls.

Parameters/mesh size		Eccentric annular channel mesh ($N \times M$)						Mesh of inner and outer cylinder walls (NSI & NSO)					
		20×20	20×25	25×25	25×30	30×25	30×30	20 & 20	20 & 25	25 & 25	25 & 30	30 & 25	30 & 30
$\overline{HF}_{i,\mathrm{ex}}^{1.I}$	Value	2.94404	2.94400	2.94622	2.94627	2.94907	2.94908	2.94671	2.94795	2.94731	2.94910	2.94616	2.94793
	% err.	0.171	0.172	0.097	0.095	0.000		0.041	0.001	0.021	0.040	0.060	
$\overline{HF}_{o,\mathrm{ex}}^{1.I}$	Value	−1.46824	−1.46820	−1.46707	−1.46704	−1.46561	−1.46560	−1.46701	−1.46740	−1.46689	−1.46753	−1.46610	−1.46672
	% err.	0.180	0.178	0.101	0.098	0.001		0.020	0.046	0.012	0.055	0.042	
$\overline{Nu}_{i,\mathrm{ex}}^{1.I}$	Value	5.05493	5.05466	5.05068	5.05061	5.04894	5.04884	5.04889	5.04856	5.04570	5.04543	5.04101	5.04076
	% err.	0.120	0.115	0.036	0.035	0.002		0.161	0.155	0.098	0.093	0.005	
$\overline{Nu}_{o,\mathrm{ex}}^{1.I}$	Value	3.51597	3.51608	3.52096	3.52103	3.52393	3.52401	3.52339	3.52670	3.52723	3.53203	3.52800	3.53273
	% err.	0.228	0.225	0.087	0.085	0.002		0.264	0.171	0.156	0.020	0.134	
$\theta_{m,\mathrm{ex}}^{1.I}$	Value	0.41759	0.41757	0.41667	0.41665	0.41590	0.41589	0.41636	0.41608	0.41588	0.41549	0.41556	0.41518
	% err.	0.409	0.403	0.187	0.183	0.003		0.284	0.217	0.169	0.075	0.092	
Time (min.)	Value	4.90300	7.64284	13.01452	21.75052	22.52500	35.34551	14.86751	15.149	16.57467	17.11302	18.23717	18.67467
	% ratio	13.872	21.623	36.821	61.537	63.728		79.613	81.122	88.755	91.638	97.657	

Table 2: Two mesh combinations in R-direction of outer and inner cylinder walls.

Parameters/mesh size		$\delta_o = 0.2,\ \delta_i = 0.1$		
		10 & 20	12 & 25	25 & 25
$\overline{HF}^{1.I}_{i,\text{ex}}$	Value	2.03697	2.03753	2.03656
	% err.	0.020	0.048	
$\overline{HF}^{1.I}_{o,\text{ex}}$	Value	−7.580 exp − 01	−7.600 exp − 01	−7.560 exp − 01
	% err.	0.316	0.462	
$\overline{Nu}^{1.I}_{i,\text{ex}}$	Value	3.37503	3.37371	3.36884
	% err.	0.184	0.145	
$\overline{Nu}^{1.I}_{o,\text{ex}}$	Value	1.91307	1.91780	1.91182
	% err.	0.065	0.313	
$\theta^{1.I}_{m,\text{ex}}$	Value	3.960 exp − 01	3.960 exp − 01	3.950 exp − 01
	% err.	0.250	0.148	
Time (min.)	Value	12.9	14	18.3
	% ratio	70.492	76.503	

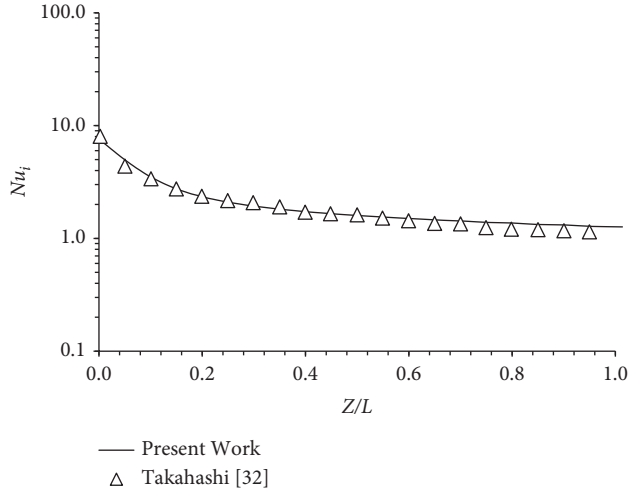

Figure 2: Results of local Nusselt number along the inner cylinder heated wall in the axial (vertical) direction compared with those of Takahashi et al. [32], $K_r = 1000$, $\chi_2 = 0.64$, $\delta_i = 0.001$, $\delta_o = 0.002$, $N = 30$, $M = 30$, NSI = 10, NSO = 20.

Thirdly, the Nusselt number for typical conventional natural convection flow averaged at outer and inner annular channel interfaces for cases 1. I and 1. O are compared with those of Mokheimer [47]. Figure 3 shows that the obtained findings agree well with those of [47].

Only representative results are presented due to space limitations. Figure 4(a) depicts the behavior of flow rate F induced in the eccentric annular channel with varying channel height L at different increasing values of the ratio of solid and fluid thermal conductivities K_r for case I. Two trends are observed for the variation of flow rate with channel height for case I. For channels with short height, when the conductivity ratio increases, the flow rate increases, and then it starts decreasing beyond a certain value of conductivity ratio. The reason is that when the conductivity ratio increases, the heat energy entering the fluid through the inner wall increases without much influence of the outer wall causing the mean bulk temperature θ_m and the buoyancy force of the annular channel fluid to increase. Consequently, the axial momentum of the fluid, which is being calculated by the axial momentum equation, increases and results in a rise in the induced flow rate into the channel. When K_r exceeds a certain value, the outer wall effect dominates with the improved thermal conductivity allowing the heat to flow in its radial and circumferential (azimuth) directions. This reduces the amount of $\overline{Q}$ and θ_m in the annular channel fluid leading to a decrease in the induced flow rate. However, for high channels ($L > 0.032$), only one trend of decreasing induced flow rate with conductivity ratio is observed. This is attributed to the rise in the thermal conductivity within the cylinder walls and a consequent reduction in $\overline{Q}$ in the fluid. The trend of having a rise in the induced flow rate up to a certain value of thermal conductivity ratio K_r and then a drop in its value is also observed in case O for a range of channel heights as shown in Figure 4(b). It means, initially, when K_r increases, the heat flow from the outer cylinder wall into the annular channel is resisted to flow through the inner insulated wall. This causes an increase in θ_m of the annular channel fluid leading to an increase the induced flow rate. Beyond a certain value of thermal conductivity ratio K_r, the heat conduction in the radial and azimuth directions within the cylinder walls become prominent, causing the heat contents in the fluid to reduce and consequently decrease the induced flow rate. Here, it is worth mentioning that greater

Table 3: Comparison with available conventional forced convection results for eccentric annular channel having linear axial increment, $K_r = 1000$, $E = 0.6$, $\chi_2 = 0.5$, $\delta_i = 0.001$, $\delta_o = 0.002$, Pr = 0.7.

Quantities/results	Current	El-Shaarawi and Haider	% err.	Current	Shah and London	% err.
$(dp/dz)_{fd}$	32.247	32.207	0.124	32.247	31.818	1.348
	Current	El-Shaarawi and Haider	% err.	Current	Trombetta	% err.
$\overline{HF}^{1.I}_{i,fd}$	3.595	3.593	0.056	3.595	3.582	0.363
$\overline{Nu}^{1.I}_{i,fd}$	5.741	5.738	0.052	5.741	5.746	0.087
$\overline{Nu}^{1.I}_{o,fd}$	4.762	4.762	0.008	4.762	4.754	0.168

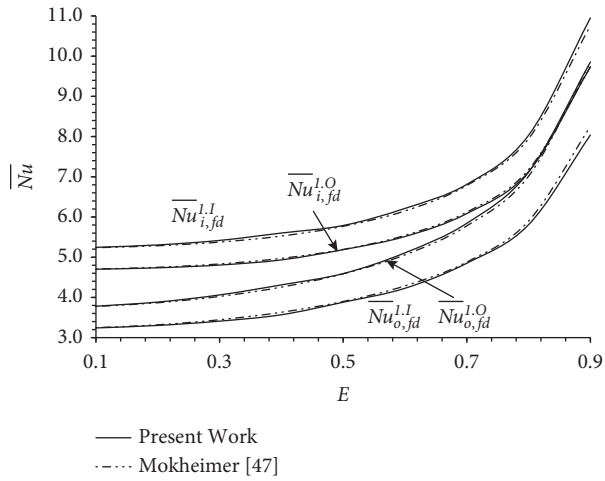

Figure 3: Present results of average Nusselt number along the outer and inner interfaces for cases 1. I and 1. O for conventional natural convection compared with those of Mokheimer [47], $K_r = 1000$, $\chi_2 = 0.5$, $\delta_o = 0.002$, $\delta_i = 0.001$, $N = 20$, $M = 20$, NSO = 25, NSI = 25.

flow rate induced in the channel in the case of convection heat transfer means a larger convective heat transfer coefficient leading to an enhanced rate of heat transfer.

Due to this variation in the trend of induced fluid flow rate, for cases I (short channels) and O (substantial range of channel heights), there is a need to determine thermal conductivity ratio K_r that induce the maximum possible flow rate for each given eccentricity E and annular channel radius ratios χ_2. These thermal conductivity ratio K_r values can be referred to as the optimum conductivity ratio $K_{r,\text{opt}}$. However, this analysis is extended to case O only since the short channels for case I do not essentially exhibit hydrodynamic and thermal full development, which may be insignificant to analyze. Four nondimensional channel heights are used for the analysis, these being 0.008, 0.01, 0.012, and 0.014. Figures 5(a) and 5(b) show the induced flow rate F plotted against the thermal conductivity ratio K_r for the four specified channel heights in a fluid annular channel ($\chi_2 = 0.5$) at $E = 0.1$ and 0.5, respectively, for case O. From these figures, it can be observed that for each channel height considered, there exists an optimum thermal conductivity ratio $K_{r,\text{opt}}$ at which maximum flow rate is induced in the annular channel. It is also observed that peak flow rates F exist over a narrow range of $K_{r,\text{opt}}$ for the four-channel heights investigated. From this observation, it can be stated that for each eccentricity, the channel height does not influence $K_{r,\text{opt}}$ significantly. This observation enables us to take the mean of the optimum thermal conductivity ratio $K_{r,\text{opt}}$ at these channel heights for each eccentricity E and plot such values against the eccentricity as shown in Figure 6. A polynomial curve of second-order is fitted to the plotted data points. It is eminent from the figure that an increase in the eccentricity in turn increases the optimum thermal conductivity ratio $K_{r,\text{opt}}$. This also means that the maximum induced flow rate for a given channel height can be achieved at larger $K_{r,\text{opt}}$ with increasing eccentricity. The values of $K_{r,\text{opt}}$ versus E are also presented in Table 4.

A similar analysis is carried out for different radius ratios at the same channel heights, i.e., 0.008, 0.01, 0.012, 0.014 for case O. Only one representative figure, i.e., Figure 7 for $\chi_2 = 0.3$ is presented here due to space constraint. This figure presents the plot of thermal conductivity ratio K_r versus the induced flow rate F for a given eccentricity $E = 0.5$. The figure depicts peak values of F existing over a narrow range of $K_{r,\text{opt}}$ for the given channel heights. Taking the mean values of the optimum thermal conductivity ratio $K_{r,\text{opt}}$ at these channel heights for each radius ratio χ_2 and plotting these values against χ_2 show an increase in $K_{r,\text{opt}}$ with χ_2 as can be seen in Figure 8. The values of $K_{r,\text{opt}}$ versus χ_2 are also presented in Table 5. Hence, these findings can help design an efficient vertical eccentric channel for effective natural convection cooling by inducing the maximum possible flow rate for given radius ratio, eccentricity, and walls thicknesses.

The cumulative heat absorbed until the channel exit $\overline{Q}$ in the annular fluid follows the same trend as for the flow rate for case O, which can be seen in Figure 9. The figure depicts the existence of peak values of $\overline{Q}$ at a range of channel heights while increasing K_r. Since F has a direct relationship

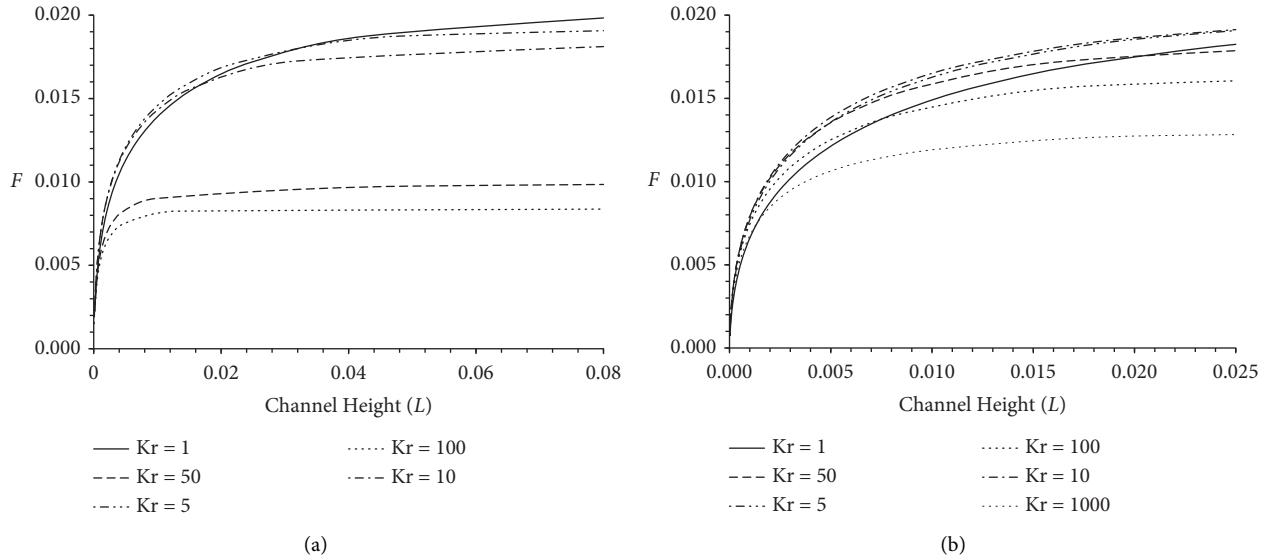

Figure 4: Induced flow rate versus channel height for different K_r, $E = 0.5$, $\chi_2 = 0.5$, $\delta_o = 0.2$, $\delta_i = 0.1$; (a) case I and (b) case O.

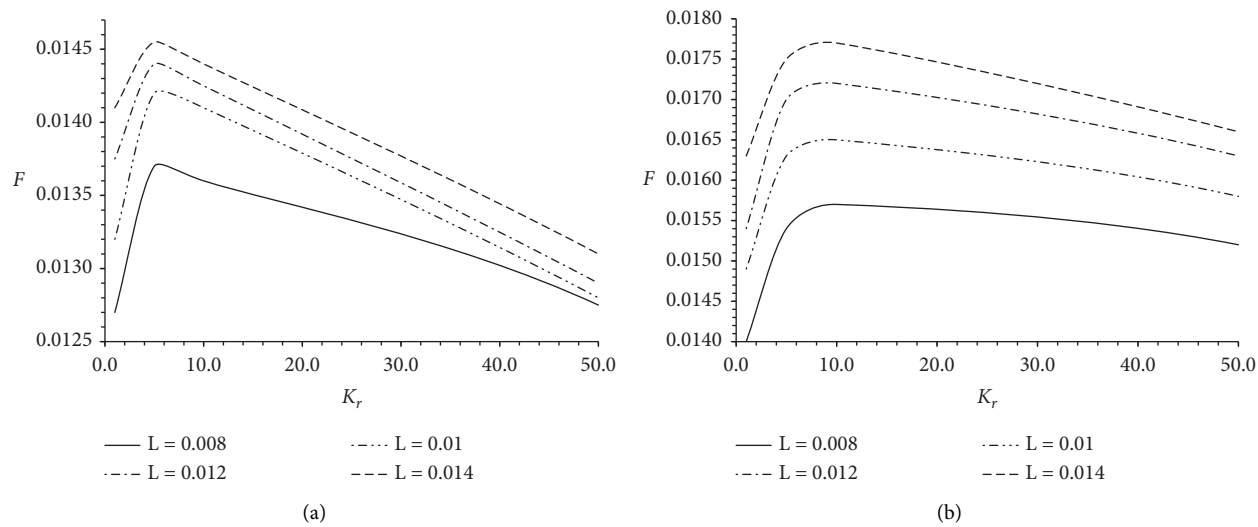

Figure 5: F vs K_r at different channel heights for case O for different eccentricities, $\chi_2 = 0.5$, $\delta_o = 0.2$, $\delta_i = 0.1$; (a) $E = 0.1$, (b) $E = 0.5$.

with $\overline{Q}$, physical interpretation can be given in a similar way as presented earlier for the induced flow rate.

In order to understand the phenomenon more, temperature profile representative results for the selected values of K_r across the channel at widest ($\psi = 0$) and narrowest gaps ($\psi = 1$) for case O are presented in Figures 10(a) and 10(b). These temperature profiles are obtained at an axial, i.e., the vertical location of 1.006×10^{-2}. An important observation is the decrease of the temperature gradient across the heated cylinder wall with conductivity ratio K_r. This is attributed to their improved thermal conductivities with K_r. In Figure 10(a), the temperature profile across the widest gap ($\psi = 0$) follows a similar pattern observed in Figure 4(b). Initially, the temperature profile goes up with K_r, but after a certain value, the profile starts to go down, the reason being the improved conduction in the inner cylinder at larger values of K_r.

Figures 11(a) and 11(b) show the flow rate variation with channel height at different cylinder walls thicknesses δ_o and δ_i for cases I and O, respectively. For case I, increasing both walls thicknesses increases the flow rate induced into the channel. This is because while the inner cylinder wall resists the heat to enter the fluid annular channel, the outer wall, which is twice as thick as the inner one with the larger surface area, prevents it from leaving the fluid annular channel. This allows the mean bulk temperature θ_m and hence the buoyancy force in the eccentric annular channel to rise. This, in turn, increases the channel flow rate. On the contrary, it is observed in Figure 11(b) for case O that when the annular channel cylinder walls become thicker, the induced flow rate F after the initial increase starts to decrease. The reason is that when the cylinder walls are thin, heat from the outer heated wall enters the fluid annular channel. As the walls

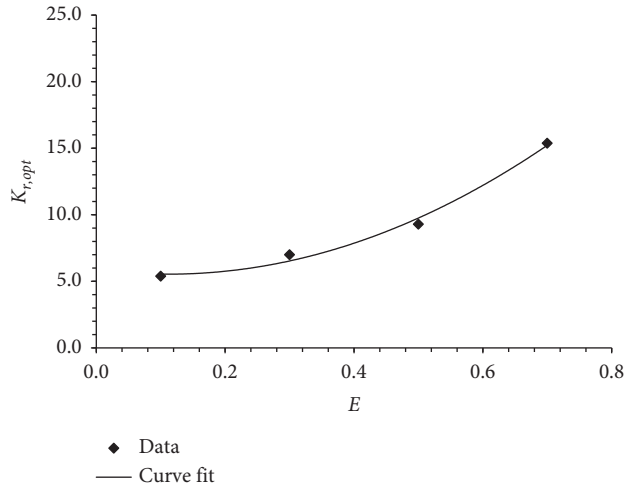

Figure 6: $K_{r,\text{opt}}$ versus E for case O, $\chi_2 = 0.5$, $\delta_o = 0.2$, $\delta_i = 0.1$.

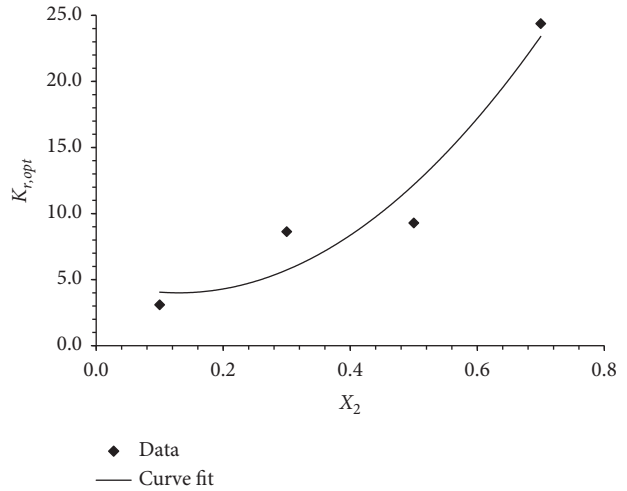

Figure 8: $K_{r,\text{opt}}$ versus χ_2 for case O, $E = 0.5$, $\delta_o = 0.2$, $\delta_i = 0.1$.

Table 4: Optimum conductivity ratio $K_{r,\text{opt}}$ at different values of eccentricity E.

E	0.1	0.3	0.5	0.7
$K_{r,\text{opt}}$	5.39	7.00	9.29	15.38

Table 5: Optimum conductivity ratio $K_{r,\text{opt}}$ at different values of radius ratio χ_2.

χ_2	0.1	0.3	0.5	0.7
$K_{r,\text{opt}}$	3.09	8.62	9.29	24.38

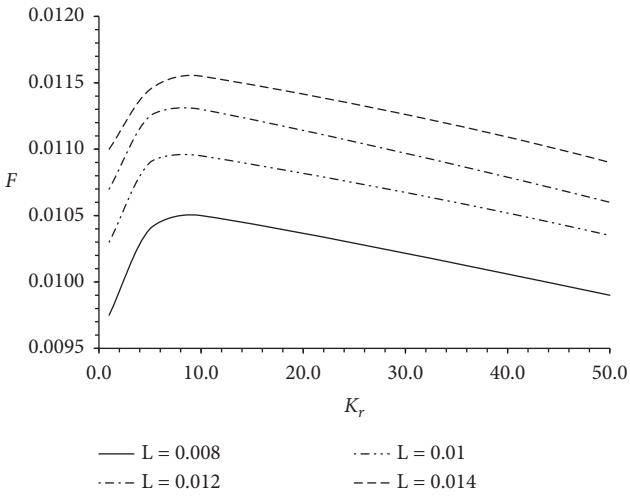

Figure 7: F vs K_r at different channel heights for case O for radius ratio $\chi_2 = 0.3$, $E = 0.5$, $\delta_o = 0.2$, $\delta_i = 0.1$.

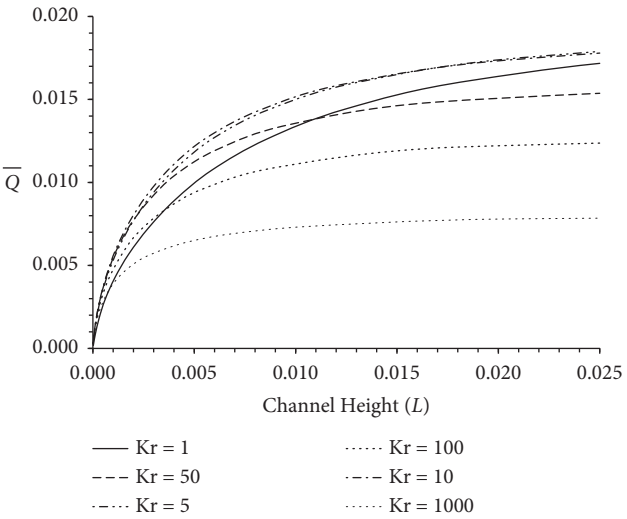

Figure 9: Total heat absorbed versus channel height for different K_r, $E = 0.5$, $\chi_2 = 0.5$, $\delta_o = 0.2$, $\delta_i = 0.1$ for case O.

thicken, the resistance of the inner insulated wall to conduct heat increases and allows more heat to be trapped in the annular channel. This causes the heat contents to increase in the fluid and hence the buoyancy force resulting in a rise in the induced flow rate into the channel. After certain thicknesses of the walls, a thick outer wall with the same nature as a wall with a low conductivity ratio resists the heat to flow through it. This consequently reduces the amount of heat reaching the annular space and hence reduces $\overline{Q}$ in the annular channel leading to a reduction in the induced flow rate.

Since the induced flow rate reversal with walls thicknesses is observed for case O (Figure 11(b)), therefore, an analysis similar to that of K_r is also carried out here for case O. The fixed relationship between δ_i and δ_o ($\delta_i = ½\ \delta_o$) is considered while presenting the results of only one wall thickness, i.e., δ_o. Figure 12 shows the variation of F with outer wall thickness δ_o at four different channel heights, i.e., 0.004, 0.006., 0.008, and 0.010, for $E = 0.5$. It is noted in this figure that for each channel height, F reaches a peak value corresponding to a specific value of δ_o. A similar variation of

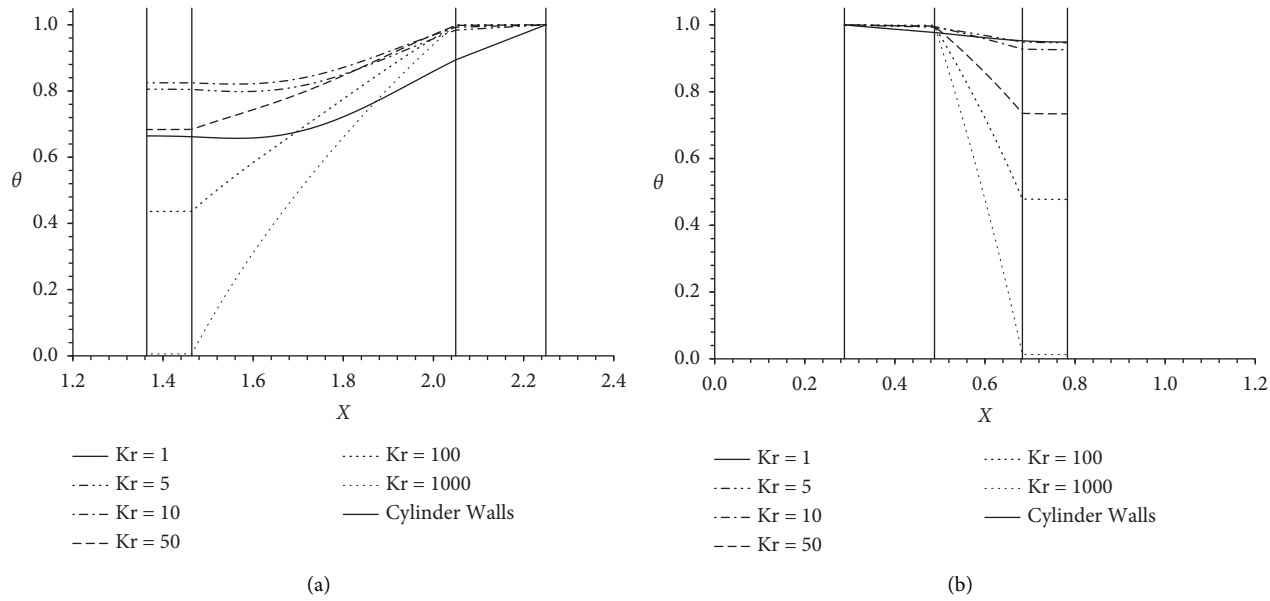

Figure 10: Temperature profiles across the channel, at the (a) widest and (b) narrowest gaps, at $Z = 1.006 \times 10^{-2}$ for different values of K_r (Case O), $E = 0.5$, $\chi_2 = 0.5$, $\delta_o = 0.2$, $\delta_i = 0.1$.

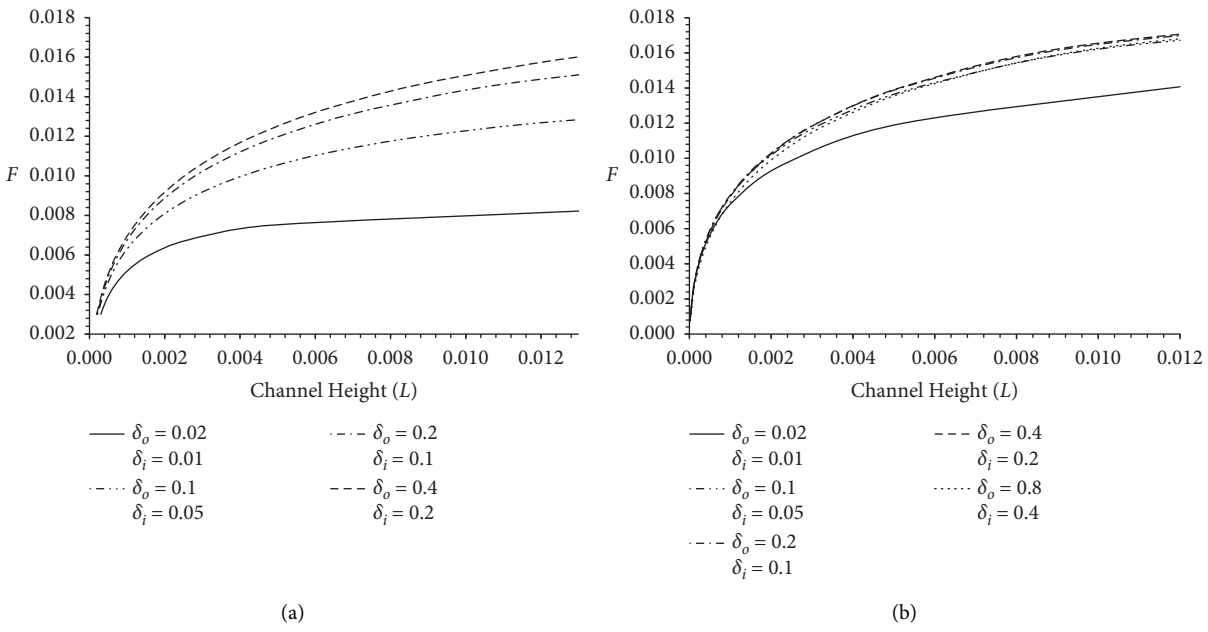

Figure 11: Induced flow rate versus channel height for different δ_o and δ_i, $K_r = 10$, $E = 0.5$, $\chi_2 = 0.5$; (a) case I and (b) case O.

F with δ_o is observed for other eccentricities. The value of δ_o with the corresponding peak value of F for each eccentricity is termed as the optimum outer wall thickness $\delta_{o,\text{opt}}$. It is also noted in the figure that peak values of F exist over a narrow range of $\delta_{o,\text{opt}}$ at different channel heights. A similar trend is observed for other eccentricities. Therefore, $\delta_{o,\text{opt}}$ is averaged at these channel heights for each eccentricity and plotted versus E as shown in Figure 13. A polynomial curve of second-order fitted to the plotted data points in the figure shows that increasing the eccentricity results in an increase in the optimum outer wall thickness $\delta_{o,\text{opt}}$. This also means that the maximum induced flow rate for a given channel height can be achieved at larger $\delta_{o,\text{opt}}$ with increasing eccentricity. The values of $\delta_{o,\text{opt}}$ versus E are also presented in Table 6. A similar analysis is carried out for different radius ratios at the same channel heights, i.e., 0.004, 0.006, 0.008, 0.01 for case O. Only one representative figure, i.e., Figure 14, shows the plot of F versus δ_o

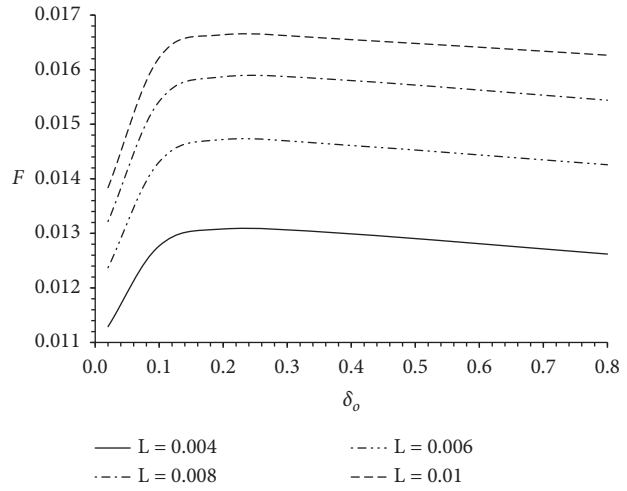

Figure 12: F vs δ_o at different channel heights for case O at $E = 0.5$, $K_r = 10$, $\chi_2 = 0.5$.

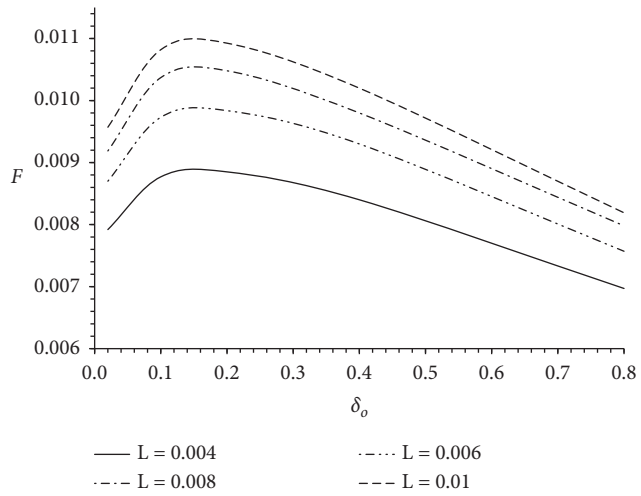

Figure 14: F vs δ_o at different channel heights for case O for radius ratio $\chi_2 = 0.3$, $K_r = 10$, $E = 0.5$.

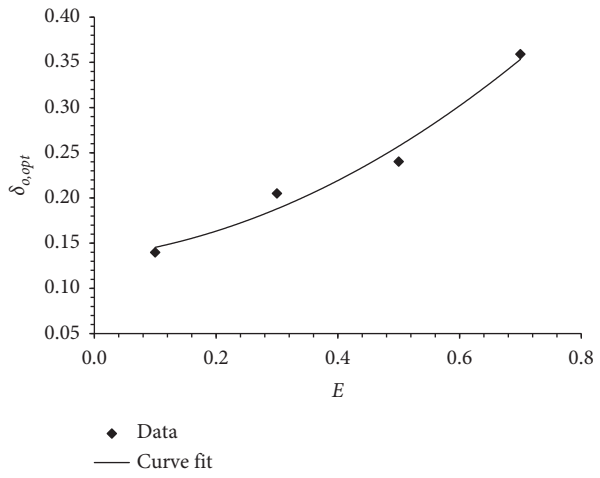

Figure 13: $\delta_{o,\text{opt}}$ versus E for case O $K_r = 10$, $\chi_2 = 0.5$.

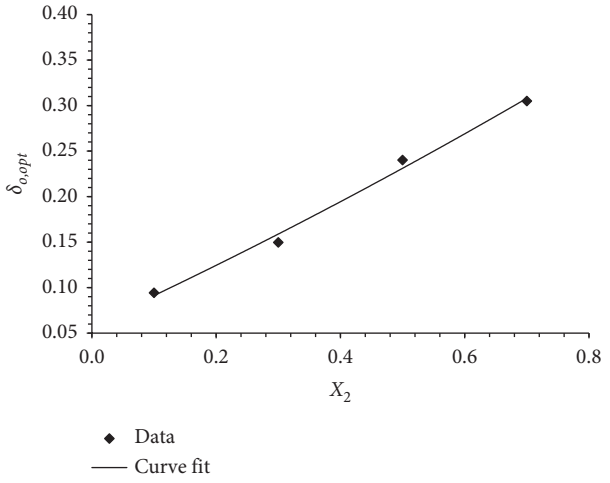

Figure 15: $\delta_{o,opt}$ versus χ_2 for case O $K_r = 10$, $E = 0.5$.

Table 6: Optimum wall thickness $\delta_{o,\text{opt}}$ at different values of eccentricity E.

E	0.1	0.3	0.5	0.7
$\delta_{o,\text{opt}}$	0.14	0.21	0.24	0.36

Table 7: Optimum wall thickness $\delta_{o,\text{opt}}$ at different values of radius ratio χ_2.

χ_2	0.1	0.3	0.5	0.7
$\delta_{o,\text{opt}}$	0.09	0.15	0.24	0.31

for a given radius ratio ($\chi_2 = 0.3$) is presented here. Figure 15 presents the mean values of $\delta_{o,\text{opt}}$ plotted versus χ_2. The plot shows increasing $\delta_{o,\text{opt}}$ with χ_2. The values of $\delta_{o,\text{opt}}$ versus χ_2 are also presented in Table 7.

Figure 16 shows the cumulative heat absorbed until the channel exit $\overline{Q}$ in the annular fluid varying with channel height at different wall thicknesses for case O. It is obvious from the figure that as the walls become thicker, the amount of $\overline{Q}$ in the fluid annular channel increases because the thick wall (inner insulated wall for case O) resists the heat to flow through it radially, which eventually traps the heat in the annular channel leading to an increase in $\overline{Q}$ and eventually enhances induced flow rate and heat transfer. However, after certain thicknesses of the walls, the amount of $\overline{Q}$ in the fluid annular channel starts decreasing. This is attributed to the less amount of heat conducted through a substantially thick outer heated cylinder wall.

The temperature profile along the symmetry line stretching across the channel is also helpful in understanding the wall thickness effect on the flow rate induction into the channel as shown in Figures 17(a) and 17(b) for case O on the widest ($\psi = 0$) and narrowest ($\psi = 1$) gap sides of the annular channel at a vertical location of 8.363×10^{-3}. It is known that thick walls resist heat flow to a greater extent

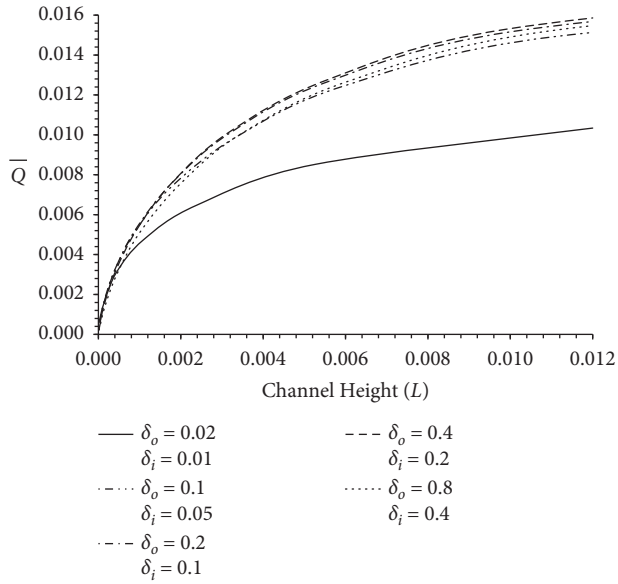

FIGURE 16: Total heat absorbed versus channel height for different δ_o and δ_i, $K_r = 10$, $E = 0.5$, $\chi_2 = 0.5$ for case O.

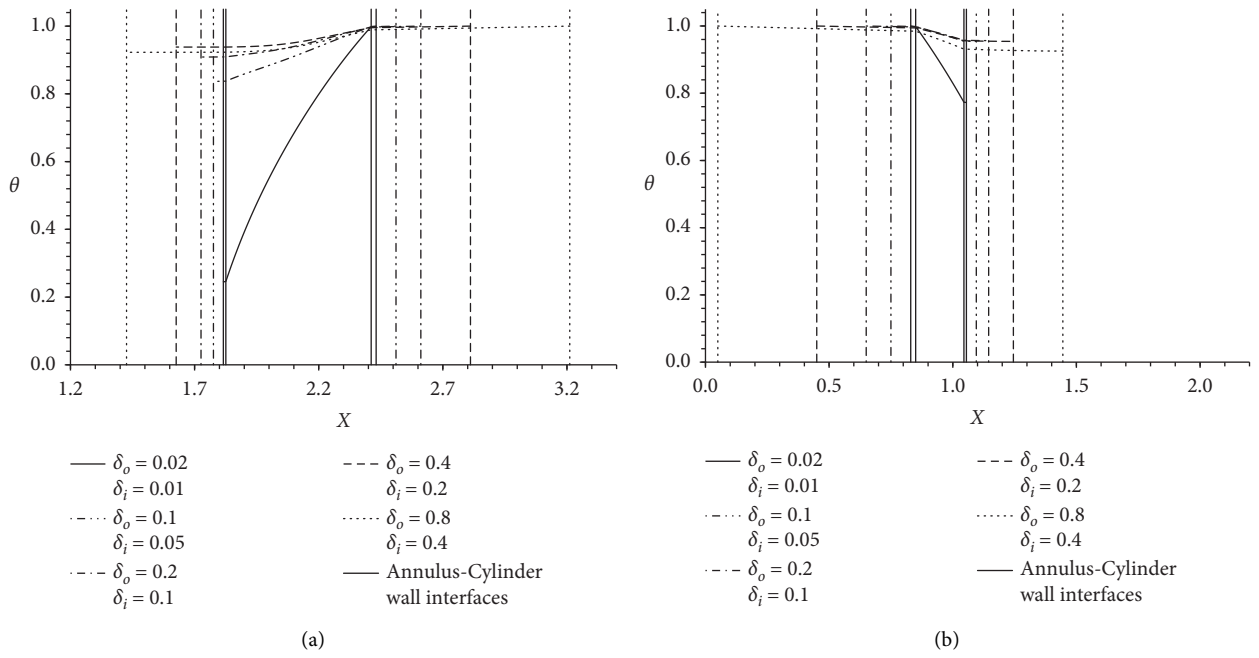

FIGURE 17: Temperature profile across the channel, at the (a) widest and (b) narrowest gaps, at an axial location of 8.363×10^{-3} for different values of δ_i and δ_o (case O), $K_r = 10$, $E = 0.5$, $\chi_2 = 0.5$.

than thin walls. However, for case O, the annular temperature profile exhibits an anomalous pattern as the cylinder walls grow in thickness, as is shown in Figures 17(a) and 17(b). The reason for this phenomenon is already given above.

5. Conclusions

Coupled conduction-laminar natural convection (conjugate) flow and heat transfer in a vertically positioned annular channel with eccentricity is numerically investigated. Numerical solution results are obtained for a Newtonian fluid with Prandtl number Pr = 0.7 in a fluid annular channel with radius ratio χ_2 and nondimensional eccentricity E each varying from 0.1 to 0.7. Commonly practiced ranges of the ratio of solid and fluid thermal conductivities ($K_r = 1$–1000) and nondimensional cylinder walls thicknesses ($\delta_o = 0.02$–0.8 and $\delta_i = 0.01$–0.4) are investigated. The effects of the ratio of solid and fluid thermal conductivities K_r and cylinder walls thicknesses δ_o and δ_i on the induced fluid flow

rate F and the cumulative heat absorbed $\overline{Q}$ in the annular fluid at different channel height is studied at various eccentricities E and annular channel radius ratios χ_2 for the boundary conditions (imposed on cylinder walls) of the third kind.

Results reveal that the induced flow rate F and the total heat absorbed $\overline{Q}$ in the annular fluid increase for case I, whereas these first increase and then decrease for case O when the thermal resistance of the cylinder walls is improved; i.e., the ratio of solid and fluid thermal conductivities is reduced or cylinder walls thicknesses are increased. It is worth mentioning that the anomalous phenomenon observed for case O may also exist in short eccentric channels for case I but not that significant. This phenomenon has, thereby, become the motive to determine the optimum thermal conductivity ratio $K_{r,\text{opt}}$ and the optimum outer wall thickness $\delta_{o,\text{opt}}$, both independent of the channel height, at which one can attain maximum induced fluid flow rate and convective heat transfer. Both $K_{r,\text{opt}}$ and $\delta_{o,\text{opt}}$ increase nonlinearly with the geometry parameters, i.e., E and χ_2. In general, the conjugate effect becomes noticeable as the thermal resistance of the cylinder walls is increased. Hence, it can be concluded that for the given geometry parameters E and χ_2 under the boundary conditions of the third kind with outer wall isothermally heated and inner wall insulated, shorter channels with suitable values of optimum thermal conductivity ratio $K_{r,\text{opt}}$ and cylinder walls thicknesses $\delta_{o,\text{opt}}$ and $\delta_{i,\text{opt}}$ can be incorporated allowing maximum F into the annular channel for effective natural convection cooling. The results of this study can be useful and can be transferred to the drilling operation in the drill rigs of oil and gas extraction. Natural convection in the idealized shear-thinning liquid mud can be useful to passively cool down the hot drill pipe within the outer wellbore wall during idle periods.

Nomenclature

a: The positive polar location of the bipolar coordinate system on the Cartesian x-axis, r_{oi} sinh η_i or r_{io} sinh η_o

e: Eccentricity (nonconcurrency of the centers of the two circular cylinders making the eccentric annular channel), $a(\coth \eta_o - \coth \eta_i)$

E: Nondimensional eccentricity, $e/(r_{io} - r_{oi})$

$(dp/dz)_{fd}$: Fully developed pressure gradient

k_f: Fluid thermal conductivity

k_s: Solid thermal conductivity of solid

K_r: Solid-fluid conductivity ratio, k_s/k_f

h: Coordinate transformation scale factor, $a/(\cosh\eta - \cos\xi)$

H: Nondimensional scale factor for coordinate transformation, h/D_h

$\overline{HF}_i$: Nondimensional heat flux averaged on the inner cylinder wall

$\overline{HF}_o$: Nondimensional heat flux averaged on the outer cylinder wall

F: Nondimensional volumetric flow rate, $F = U_o(1 - \chi_2^2)$

Gr$*$: Modified Grashof number, Gr D_h/l

i: η-direction bipolar grid and R-direction cylindrical grid index

j: ξ-direction bipolar grid and ϕ-direction cylindrical grid index

L: Nondimensional height of vertical annular channel (value of Z at channel exit), l/Gr^*

NSI: R-direction inner cylinder wall intervals

NSO: R-direction outer cylinder wall intervals

Nu_i: Localized Nusselt number for the inner solid-fluid interface

$\overline{Nu}_i$: Nusselt number averaged on the inner cylinder wall

$\overline{Nu}_o$: Nusselt number averaged on the outer cylinder wall

P: Nondimensional fluid Pressure gradient inside the annular channel at any cross-section, $(P'D_h^4)/(\rho l^2 \gamma^2 \text{Gr}^{*^2})$

$\overline{Q}$: Nondimensional cumulative heat absorbed until the annular channel exit, i.e., values of Q at $z = l$, $F\theta_{m,ex}$

M: ξ- and ϕ-directions intervals in the annular channel and cylinder walls, respectively

N: η-direction intervals in the annular channel

R: First transverse cylindrical coordinate (radial)

ΔR_i: $(\chi_2 - \chi_1)/\text{NSI}$

ΔR_o: $(\chi_4 - \chi_3)/\text{NSO}$

r_{ii}: Radius of the inner surface of the inner cylinder

r_{oi}: Radius of the outer surface of the inner cylinder

r_{io}: Radius of the inner surface of the outer cylinder

r_{oo}: Radius of the outer surface of the outer cylinder

T_o: Fluid temperature at the annular channel entrance

T_w: Temperature of the isothermally heated wall

V: Nondimensional η-velocity component, vD_h/γ

u_o: Entrance or average (mean) axial velocity, $\overline{u}$

U_o: Nondimensional velocity in the axial direction at annular channel entrance, $(u_o r_{io}^2)/(l\gamma \text{Gr}^*)$

U: Nondimensional velocity in the axial direction at any point, $(ur_{io}^2)/(l\gamma \text{Gr}^*)$

W: Nondimensional velocity component in ξ-direction, wD_h/γ

Z: Nondimensional coordinate in the axial direction, $z/(l\text{Gr}^*)$

ΔZ: Nondimensional step increment in the axial direction, $\Delta z/(l\text{Gr}^*)$

Greek Letters

η_i: η value on the inner annular channel interface,

η_o: η value on the outer annular channel interface

β: Coefficient of volumetric thermal expansion

η: First bipolar coordinate in the transverse direction inside the *annular channel*

$\Delta\eta$: Mesh size of the numerical grid in η-direction, $(\eta_i - \eta_o)/N$

θ: Nondimensional temperature, $(T - T_o)/(T_w - T_o)$ for isothermal walls case

ψ: Normalized value of ξ, ξ/π

ϕ: Second transverse cylindrical coordinate (tangential)
δ_i: Inner cylinder wall nondimensional thickness, $\chi_2 - \chi_1$
δ_o: Outer cylinder wall nondimensional thickness, $\chi_4 - \chi_3$
χ_1: Ratio of r_{ii} and r_{io}, r_{ii}/r_{io}
χ_2: Ratio of r_{oi} and r_{io} (radius ratio of the eccentric annular channel), r_{oi}/r_{io}
χ_3: Nondimensional radius of the inner surface of the outer cylinder, $r_{io}/r_{io} = 1$
χ_4: Ratio of r_{oo} and r_{io}, r_{oo}/r_{io}
ξ: Second bipolar coordinate in the transverse direction inside the annular channel.

Data Availability

The conjugate natural convection data used to support the findings of this study have been deposited in the Figshare repository (https://figshare.com/articles/dataset/Conjugate_Natural_Convection_Heat_Transfer/16929766).

Conflicts of Interest

There are no conflicts of interest regarding the publication of this paper.

Acknowledgments

Acknowledgments are due to Jubail University College, Royal Commission for Jubail.

References

[1] N. K. Anand and D. R. Tree, "Some studies of the effects of axial conduction in a tube wall on the steady-state laminar convective heat transfer," *Journal of Heat Transfer*, vol. 109, no. 4, pp. 1025–1028, 1987.

[2] S. H. Kim, N. K. Anand, and W. Aung, "Effect of wall conduction on free convection between asymmetrically heated vertical plates: uniform wall heat flux," *International Journal of Heat and Mass Transfer*, vol. 33, no. 5, pp. 1013–1023, 1990.

[3] D. Huu Chung, "Conjugate natural convection of a power law fluid in a vertical finite thick channel with heat sources," *International Journal of Numerical Methods for Heat and Fluid Flow*, vol. 7, no. 2/3, pp. 200–214, 1997.

[4] M. A. Sheremet, "Three-dimensional conjugate natural convection in a vertical cylinder under heat transfer to the surroundings," *Fluid Dynamics*, vol. 46, no. 4, pp. 647–657, 2011.

[5] M. A. Hassab, M. K. Mansour, and M. S. Ismail, "The effect of axial wall conduction on heat transfer parameters for a parallel-plate channel having a step change in boundary conditions," *Numerical Heat Transfer, Part A: Applications*, vol. 63, no. 6, pp. 430–451, 2013.

[6] M. A. I. El-Shaarawi, M. A. Al-Nimr, and M. A. Hader, "Transient conjugated heat transfer in concentric annuli," *International Journal of Numerical Methods for Heat and Fluid Flow*, vol. 5, no. 5, pp. 459–473, 1995.

[7] M. A. I. El-Shaarawi, M. A. Al-Nimr, and M. M. K. Al Yah, "Transient Conjugate heat transfer in a porous medium in concentric annuli," *International Journal of Numerical Methods for Heat and Fluid Flow*, vol. 9, no. 4, pp. 444–460, 1999.

[8] M. A. I. El-Shaarawi and A. A. A. Negm, "Conjugate natural convection heat transfer in an open-ended vertical concentric annulus," *Numerical Heat Transfer, Part A: Applications*, vol. 36, no. 6, pp. 639–655, 1999.

[9] M. A. I. El-Shaarawi and A. A. A. Negm, "Transient combined natural convection-conduction in open-ended vertical concentric annuli," *Heat and Mass Transfer*, vol. 35, no. 2, pp. 133–141, 1999.

[10] T. K. Aldoss, M. Alkam, and M. Shatarah, "Natural convection from a horizontal annulus partially filled with porous medium," *International Communications in Heat and Mass Transfer*, vol. 31, no. 3, pp. 441–452, 2004.

[11] H. Imtiaz and F. M. Mahfouz, "Conjugate heat transfer within a concentric annulus filled with micropolar fluid," *Heat and Mass Transfer*, vol. 50, no. 4, pp. 457–468, 2014.

[12] A. I. Alsabery, K. Naganthran, F. M. Azizul, I. Hashim, and R. Nazar, "Numerical study of conjugate natural convection heat transfer of a blood filled horizontal concentric annulus," *International Communications in Heat and Mass Transfer*, vol. 114, Article ID 104568, 2020.

[13] M. L. Trombetta, "Laminar forced convection in eccentric annuli," *International Journal of Heat and Mass Transfer*, vol. 14, no. 8, pp. 1161–1173, 1971.

[14] M. Singh and S. C. Rajvanshi, "Heat transfer between eccentric rotating cylinders," *Journal of Heat Transfer*, vol. 102, no. 2, pp. 347–350, 1980.

[15] E. E. Feldman, R. W. Hornbeck, and J. F. Osterle, "A numerical solution of laminar developing flow in eccentric annular ducts," *International Journal of Heat and Mass Transfer*, vol. 25, no. 2, pp. 231–241, 1982.

[16] E. E. Feldman, R. W. Hornbeck, and J. F. Osterle, "A numerical solution of developing temperature for laminar developing flow in eccentric annular ducts," *International Journal of Heat and Mass Transfer*, vol. 25, no. 2, pp. 243–253, 1982.

[17] M. A. I. El-Shaarawi, H. I. Abualhamayel, and E. M. A. Mokheimer, "Developing laminar forced convection in eccentric annuli," *Heat and Mass Transfer*, vol. 33, no. 5-6, pp. 353–362, 1998.

[18] M. A. I. El-Shaarawi and E. M. A. Mokheimer, "Free convection in vertical eccentric annuli with a uniformly heated boundary," *International Journal of Numerical Methods for Heat and Fluid Flow*, vol. 8, no. 5, pp. 488–503, 1998.

[19] M. A. I. El-Shaarawi and E. M. A. Mokheimer, "Developing free convection in open-ended vertical eccentric annuli with isothermal boundaries," *Journal of Heat Transfer*, vol. 121, no. 1, pp. 63–72, 1999.

[20] C. Shu, Q. Yao, K. S. Yeo, and Y. D. Zhu, "Numerical analysis of flow and thermal fields in arbitrary eccentric annulus by differential quadrature method," *Heat and Mass Transfer*, vol. 38, no. 7-8, pp. 597–608, 2002.

[21] C. Shu and Y. L. Wu, "Domain-free discretization method for doubly connected domain and its application to simulate natural convection in eccentric annuli," *Computer Methods in Applied Mechanics and Engineering*, vol. 191, no. 17-18, pp. 1827–1841, 2002.

[22] W. L. Wu, C. Shu, J. Qiu, and J. Tani, "Implementation of multigrid approach in domain-free discretization method to speed up convergence," *Computer Methods in Applied Mechanics and Engineering*, vol. 192, no. 20-21, pp. 2425–2438, 2003.

[23] E. M. A. Mokheimer and M. El-Shaarawi, "Maximum possible induced flow rates in open-ended vertical eccentric annuli with uniform heat flux," *International Journal of Numerical Methods for Heat and Fluid Flow*, vol. 15, no. 2, pp. 161–182, 2005.

[24] E. M. A. Mokheimer and S. Sami, "Conditions for pressure build-up due to buoyancy effects on forced convection in vertical

eccentric annuli under thermal boundary condition of first kind," *Heat and Mass Transfer*, vol. 43, no. 2, pp. 175–189, 2006.

[25] B. A. Harab, T. Calisir, and S. Baskaya, "Numerical investigation of transient natural convection heat transfer of non-Newtonian nanofluids between eccentric annulus," *Arabian Journal for Science and Engineering*, vol. 44, no. 6, pp. 5631–5646, 2019.

[26] M. A. I. El-Shaarawi and S. A. Haider, "Critical conductivity ratio for conjugate heat transfer in eccentric annuli," *International Journal of Numerical Methods for Heat and Fluid Flow*, vol. 11, no. 3, pp. 255–279, 2001.

[27] M. A. I. El-Shaarawi, E. M. A. Mokheimer, and A. Jamal, "Conjugate effects on steady laminar natural convection heat transfer in vertical eccentric annuli," *International Journal for Computational Methods in Engineering Science and Mechanics*, vol. 6, no. 4, pp. 235–250, 2005.

[28] M. A. I. El-Shaarawi, E. M. A. Mokheimer, and A. Jamal, "Geometry effects on conjugate natural convection heat transfer in vertical eccentric annuli," *International Journal of Numerical Methods for Heat and Fluid Flow*, vol. 17, no. 5, pp. 461–493, 2007.

[29] A. Jamal, M. A. I. El-Shaarawi, and E. M. A. Mokheimer, "Critical conductivity ratio and wall thickness for conjugate natural convection heat transfer in vertical eccentric annuli," *Numerical Heat Transfer, Part A: Applications*, vol. 59, no. 9, pp. 719–737, 2011.

[30] D. Nasiri, A. A. Dehghan, and M. R. Hadian, "Conjugate natural convection between horizontal eccentric cylinders," *Heat and Mass Transfer*, vol. 53, no. 3, pp. 799–811, 2017.

[31] M. S. El-Genk and D. V. Rao, "Buoyancy induced instability of laminar flows in vertical annuli-I. Flow visualization and heat transfer experiments," *International Journal of Heat and Mass Transfer*, vol. 33, no. 10, pp. 2145–2159, 1990.

[32] K. Takahashi, T. Morikawa, Y. Harada, and N. Hattori, "Natural convective heat transfer in uniformly heated vertical pipe annuli," *Heat Transfer - Asian Research*, vol. 30, no. 8, pp. 676–688, 2001.

[33] R. Hosseini, M. R. Heyrani-Nobari, and M. Hatam, "An experimental study of heat transfer in an open-ended vertical eccentric annulus with insulated and constant heat flux boundaries," *Applied Thermal Engineering*, vol. 25, no. 8-9, pp. 1247–1257, 2005.

[34] S. Husain and M. A. Siddiqui, "Experimental and numerical analyses of natural convection flow in a partially heated vertical annulus," *Numerical Heat Transfer, Part A: Applications*, vol. 70, no. 7, pp. 763–775, 2016.

[35] V. K. Chithrakumar, G. Venugopal, and M. R. Rajkumar, "Convection in vertical annular gap formed by stationary heated inner cylinder and rotating unheated outer cylinder," *Heat and Mass Transfer*, vol. 55, no. 10, pp. 2873–2888, 2019.

[36] T. Zhu, Z. Jia, and X. Wang, "Experimental and simulation study of forced convection in vertical eccentric annular space," *International Journal of Thermal Sciences*, vol. 161, Article ID 106735, 2021.

[37] W. F. Hughes and E. W. Gaylord, *Basic Equations of Engineering Science*, Schaum Outline Series, New York, NY, USA, 1964.

[38] M. A. I. El-Shaarawi and M. A. Al-Nimr, "Fully developed laminar natural convection in open-ended vertical concentric annuli," *International Journal of Heat and Mass Transfer*, vol. 33, no. 9, pp. 1873–1884, 1990.

[39] M. A. I. El-Shaarawi and M. A. Al-Attas, "Unsteady natural convection in open-ended vertical concentric annuli," *International Journal of Numerical Methods for Heat and Fluid Flow*, vol. 2, pp. 503–516, 1992.

[40] A. I. M. El-Shaarawi and A. M. Al-Attas, "Transient induced flow through a vertical annulus," *JSME International Journal Series B*, vol. 36, no. 1, pp. 156–165, 1993.

[41] M. A. Al-Nimr and M. A. I. El-Shaarawi, "Analytical solution for transient laminar fully developed free convection in vertical channels," *Heat and Mass Transfer*, vol. 30, no. 4, pp. 241–248, 1995.

[42] M. A. I. El-Shaarawi, E. M. A. Mokheimer, and H. I. Abulhamayel, "Limiting values for free-convection induced flow rates in vertical eccentric annuli with an isothermal boundary," *Numerical Heat Transfer: Applications*, vol. 39, no. 6, pp. 611–630, 2001.

[43] F. T. Akyildiz, A. F. A. AlSohaim, and N. Kaplan, "Electro-osmotic and pressure-driven flow in an eccentric micro-annulus," *Zeitschrift für Naturforschung A*, vol. 74, no. 6, pp. 513–521, 2019.

[44] M. L. Nayyar, *Piping Handbook*, McGraw-Hill, New York, NY, USA, 7th edition, 2000.

[45] M. A. I. El-Shaarawi, *Heat transfer and hydrodynamics in the entrance region of concentric annuli with stationary and rotating inner walls*, PhD thesis, University of Leeds, Leeds, UK, 1974.

[46] R. K. Shah and A. L. London, *Laminar Flow Forced Convection in Ducts*, Academic Press, New York, NY, USA, 1978.

[47] E. M. A. Mokheimer, *Heat transfer in eccentric annuli*, PhD thesis, King Fahd University of Petroleum and Minerals, Dhahran, Saudi Arabia, 1996.